Journal of Materials Science: Materials in Electronics (2018) 29:19413–19424
https://doi.org/10.1007/s10854-018-0070-5

Development of tungsten disulfide ZnO nanohybrid photocatalyst for organic pollutants removal

Arulappan Durairaj[1] · Daniel Lydia Jennifer[1] · Thangavel Sakthivel[2] · Asir Obadiah[1] · Samuel Vasanthkumar[1]

Received: 17 July 2018 / Accepted: 17 September 2018 / Published online: 18 September 2018

Abstract
In this study, ZnO and ZnO/WS_2 nanohybrid were synthesized by a facile microwave approach. Nanohybrid phase purity and structural features were examined through XRD, SEM–EDS, and EDS color mapping techniques. The optical absorbance and band gap energy of the ZnO/WS_2 nanohybrid was measured by the UV–DRS. Functional group features on the ZnO/WS_2 nanohybrid was investigated by the FT-IR spectroscopy. Further, the position of the conduction band and conductivity of the prepared ZnO/WS_2 nanohybrid was studied by the Mott–Schottky and Nyquist plot techniques. The photocatalytic properties of the ZnO/WS_2 nanohybrid were evaluated through the degradation of anionic and cationic organic pollutants such as methylene blue, bromophenol-B and 4-nitrophenol respectively. The organic pollutants degradation efficiency was determined by the UV absorbance spectroscopy and HPLC. Pseudo first order rate constant of the degradation reaction was calculated by the Langmuir–Hazelwood kinetic model. In addition, probe molecule mineralization was evaluated by TOC analysis. The ZnO/WS_2 nanohybrid catalysts durability was analyzed by subjecting it to four repeated photocatalytic cycles. After the photocatalysis reaction the catalyst structure distortion was analyzed by the XRD technique.

1 Introduction

Photocatalytic chemical reactions are cost effective and environmental friendly, since they are purely driven by natural sun light and a semiconductor. After the first invention of photocatalytic water splitting using TiO_2 under UV light, this technique has been widely utilized in energy production and environmental remediation fields [1]. It is well known that, the natural incoming irradiation from sun light contains, large quantum of visible photons in comparison to UV photons. Considering, these aspects, researchers are focusing to develop a visible light active catalyst. In this direction, plenty of visible-light active photocatalysts that have been tried during the past few decades, include single, binary, ternary, metal oxides and sulfides [2]. However, the accessible visible-light photocatalyst efficiency has not reached the required level. The efficiency decrement could be ascribed to several factors, among which the rapid photon induced charge carrier recombination process is crucial. Tremendous efforts have been made to prevent the charge carrier recombination in photocatalysis. In this regard, two-dimensional sheets like nanostructures were suggested to be promising candidate since, such a material strongly prevents the electron–hole recombination due to their high electron affinity [3].

Nanostructured semiconductor hybrid photocatalyst research has attracted much attention due to their widespread application [4]. After the discovery of graphene, two-dimensional nanostructures based research has gained more visibility in different sectors. Graphene is a widely studied nanostructure for usage in semiconductor hybrid photocatalysis [5]. After the construction of graphene-semiconductor as a hybrid, the efficiency was found to improve multi fold. The efficiency increment was possible through the inhibition of photo electron–hole recombination, improved photon harvesting and availability of more active sites. Several articles reported the intensive study of these phenomena in various graphene-semiconductor nano hybrids systems [6]. However, the main concern was the stability of graphene

✉ Samuel Vasanthkumar
kumar2359@yahoo.com

[1] Departmentof Chemistry, Karunya Institute of Technology and Sciences, Karunya Nagar, Coimbatore, Tamil Nadu 641-114, India

[2] Key Lab of Advanced Transducers and Intelligent Control System, Ministry of Education and Shanxi Province, College of Physics and Optoelectronics, Taiyuan University of Technology, Taiyuan 030024, People's Republic of China

in the presence of hydroxyl radical. Photocatalyst reactions mainly produce OH radicals, which destroy the pollutants as well as the graphene. Therefore, the graphene structure fragmentation occurs which leads to decline in it is efficiency [7]. The poor stability of the graphene as a semiconductor nanohybrid photocatalyst encouraged us, to develop a novel two-dimensional nanostructured semiconductor hybrid photocatalyst. In this context, graphene analogs such as molybdenum disulfide (MoS_2), graphitic carbon nitride (g-C_3N_4) based semiconductor nanohybrid structures were fabricated and their photocatalytic properties were examined [8, 9].

Recently, transition metal chalcogenides has been the focus of research, as an alternative to graphene nanohybrid photocatalyst due to their intriguing physical and photochemical properties. The transition metal chalcogenides-semiconductor nanohybrid photocatalytic properties have been studied by different research groups [10]. The study brought to light the fact that, the efficiency of the nanohybrid catalyst was increased when compared with the bare catalyst owing to their high surface area, electronic conductivity and electron affinity. In this scenario, several transition metal chalcogenides were suggested for fabrication of semiconductor nanohybrid photocatalyst [11, 12]. Among them, tungsten disulfide (WS_2) attracted more attention due to their, high surface area, better optical absorbance and suitable valence–conduction band potential. In addition to these properties, the narrow band-gap of WS_2 creates rapid electron–hole recombination there by decreasing its efficiency [13, 14].

ZnO is a promising and broadly studied candidate in semiconductor photocatalytic field. ZnO exhibits high photocatalytic activity due to their high electron mobility, which is nearly twofold higher than TiO_2 [15, 16]. This enhanced electron mobility increased its life time as the charge carrier. However, ZnO can active under UV light due to their large band gap and also rapid electron–hole recombination strongly discourages to use it as a photocatalyst [17, 18]. To overcome the above deficiency in ZnO, it was fabricated as a hybrid with two-dimensional materials, including graphene, graphdiyne, MoS_2 and g-C_3N_4 [6, 19–21]. Therefore, our objective was to develop a novel WS_2/ZnO nanohybrid photocatalyst. The photocatalytic activity was examined by employing it for the degradation of methylene blue (MB), bromophenol-B (BPB) and 4-nitrophenol (4-NP). In addition, the organic molecule mineralization efficiency of WS_2/ZnO nanohybrid photocatalyst was evaluated against MB by the total organic carbon (TOC) removal technique. Further, a plausible mechanism is proposed for the enhanced efficiency. The UV–DRS, Nyquist plot and photoluminescence (PL) spectra investigation strengthens the proposed mechanism.

2 Materials and methods

2.1 Materials

Zinc sulfate ($ZnSO_4$), sodium hydroxide (NaOH) and tungsten sulphide (WS_2) were purchased from Sigma-Aldrich, India. MB ($C_{16}H_{18}ClN_3S$), ethyl alcohol (EtOH), BPB ($C_{19}H_{10}Br_4O_5S$), 4-NP ($C_6H_5NO_3$), tertiary butyl alcohol (t-BuOH) and EDTA disodium salt [$CH_2N(CH_2COOH)CH_2COONa]2H_2O$ was purchased from Merck chemicals, India. All the reactions were carried out using double distilled (DD) water. All the chemicals were used as obtained without any further purification.

2.2 Preparation of ZnO and ZnO–WS_2 nanohybrid

At first, the procured WS_2 was subjected to sonication to get an exfoliate WS_2. The ZnO/WS_2 nanohybrid and ZnO were synthesized through facile microwave techniques. Certain amount of zinc sulfate was dissolved in DD water and subsequently sonicated for 10 min to make a homogenous solution. Afterwards, the solution was irradiated with microwave by adding NaOH solution for every 30 s. Later on the mixture was again irradiated with microwave by addition of ethanolic WS_2 drop wise for every 30 s. After completion of the reaction, the precipitate was collected, centrifuged and washed several times with copious amount of water and alcohol. The collected ZnO/WS_2 nanohybrid was dried overnight at 80 °C. Likewise, different (5, 10 & 20) wt% of WS_2 loaded ZnO/WS_2 nanohybrid were prepared by the same procedure. The obtained nanohybrids were used for the characterization and the photocatalytic studies. For comparison, pure ZnO was also synthesized by the microwave technique and used.

2.3 Characterization

The phase purity and structure of ZnO, WS_2 and ZnO/WS_2 nanohybrid were analyzed by X-ray diffractometer (Shimadzu model: XRD 6000 with Cu Kα radiation) in the range of 5°–80°. To determine the morphological aspects and elemental distribution of the prepared materials, they were analyzed using a scanning electron microscope (SEM) (Model: JOEL JSM-6390 Hitachi S-4500) equipped with energy dispersive X-ray spectroscopy (EDS). Identification of the functional groups in the ZnO/WS_2 nanohybrid was carried out using a Fourier transformed infrared (FT-IR) spectrometer. The absorbance and the band gap of the prepared composite were analyzed by a UV–DRS spectrometer (Shimadzu, Japan). $BaSO_4$ is used as the reference material. Flat band potential and electrochemical impedance analysis

was measured using a CHI-600D electrochemical instrument. Room temperature PL spectra were analyzed with the PL spectrometer FLUOROLOG, HORIBAYVON. The photocatalytic activity was measured with respect to the MB and BPB degradation as sample molecules. The photocatalytic dye degradation efficiency was measured using the UV absorbance spectroscopy (Model: JASCO V-670). High-performance liquid chromatography analysis was carried out using a Shimadzu (LC-20AD) with a S-18 column to study the MB degradation. The dye molecules mineralization was analyzed by the TOC removal technique using a Shimadzu, TOC-VLPH instrument.

2.4 Photocatalytic measurement

To determine the photocatalytic activity of ZnO/WS_2 nanohybrid and the synthesized ZnO, both were tested against the degradation of MB, BPB and 4-NP which were representative organic pollutant molecules. At first, 5 mg of the catalyst was dispersed in DD water and subjected in sonication. Then, 50 ml of probe organic molecule (1×10^{-5} M) was added into the catalytic solution. The mixture was stirred without any interruption to reach the adsorption equilibrium in about 1 h. Then, 5 ml of the solution was taken from the equilibrium mixture and it was centrifuged to separate the catalyst from the mixture. The catalyst free probe solution absorbance was measured by using a UV-spectrometer at the MB maximum absorbance wavelength of 664 nm. Subsequently, the mixture was placed in a homemade photocatalytic reactor. The solution was irradiated under visible light with a maximum emission of $\lambda > 385$ nm with a 6 W power supplier. In periodic intervals of time, 5 ml of the reaction solution was taken from the mixture, and it was centrifuged. The absorbance of the supernatant solution was measured using a UV-spectrophotometer. The organic molecule photocatalytic degradation efficiency was calculated by the following expression

$$\text{Degradation efficiency (DE \%)} = \left(1 - \frac{C_t}{C_0}\right) \times 100 \quad (1)$$

Here C_0 and C_t refer to the initial and time dependent concentration of the target molecule. Further, the photocatalytic degradation reaction follows the pseudo-first order rate kinetics provided by Langmuir–Hazlewood model kinetics [22]. The plot between irradiation duration against dye concentration changes (C_t/C_0) ratio was linear. The slope of the linear curve expresses the pseudo-first order rate constant.

$$\text{Pseudo first order rate constant } \ln\left(\frac{C}{C_0}\right) = -kt \quad (2)$$

Here, 't' denotes to the reaction time and 'k' is the pseudo first order rate constant. The organic molecule mineralization during the photocatalysis was measured by the TOC removal technique in periodic intervals. The fresh sample organic molecule TOC was measured as the initial (TOC_0) concentration, during the photocatalytic reaction the measured TOC concentration at different periodic intervals of time (t) is denoted as (TOC_t). The mineralization efficiency of the photocatalytic reaction is calculated using the below expression

$$\text{Mineralization efficiency (\%)} = \left[1 - \left(\frac{TOC_t}{TOC_0}\right)\right] \times 100 \quad (3)$$

The recyclability of ZnO/WS_2 nanohybrid was determined, to understand the repeated use of the catalyst. Once MB dye was completely degraded, the ZnO/WS_2 nanohybrid was isolated by centrifugation. Then the isolated ZnO/WS_2 photocatalyst was washed with water and further dried in an oven to eliminate the moisture. Then, the same catalyst was reused for the photocatalytic degradation reaction of fresh MB. The above procedure was repeated four times. To determine the structural stability of the ZnO/WS_2 nanohybrid, after the repeated photocatalytic reaction, the catalyst structure was examined by XRD and compared with the freshly prepared nanohybrid material.

3 Result and discussion

The phase and crystal structure of the ZnO, WS_2 and ZnO/WS_2 nanohybrid was characterized by X-ray diffraction technique. Figure 1 represents the XRD pattern of ZnO, WS_2 and ZnO/WS_2 nanohybrid. The ZnO exhibits the diffraction peaks at 31.8°, 34.5°, 36.3°, 47.6°, 56.7° and 63°. The XRD peaks correlated well with the peaks obtained for hexagonal wurtzite ZnO with the JCPDS number (36-1451). The diffraction patterns are well matched with the Miller planes of (100), (002), (101), (102), (110) and (103) [23]. The calculated d spacing was 2.59 Å and the determined grain size was 2.78 nm for ZnO. Further, the XRD pattern of 2H–WS_2 exhibited eight different peaks at 14.3°, 28.9°, 33.5°, 35.9°, 39.5°, 44°, 49.7°, 55.9° and 58.4°. The diffraction peaks correspond to the reflection of planes (002), (004), (101), (102), (103), (006), (105), (106) and (110) respectively. All the peaks are clearly well matched with 2H–WS_2—JCPDS number (84-1398). WS_2 has a multilayered 2D structure owing to the presence of (002), (101) and (110) planes [24]. Figure 1 (top) shows the XRD pattern of freshly prepared ZnO/WS_2 nanohybrid. The XRD pattern showed peaks at 14.3°, 31.8°, 34.5°, 36.3°, 47.6° and 63°. On comparison it is understood that these values correspond to major peaks of 2H–WS_2 and ZnO phase. The calculated d spacing and grain size was 2.61 Å and 2.87 nm respectively for ZnO/WS_2. The XRD results indicate that the ZnO/WS_2 nanohybrid was

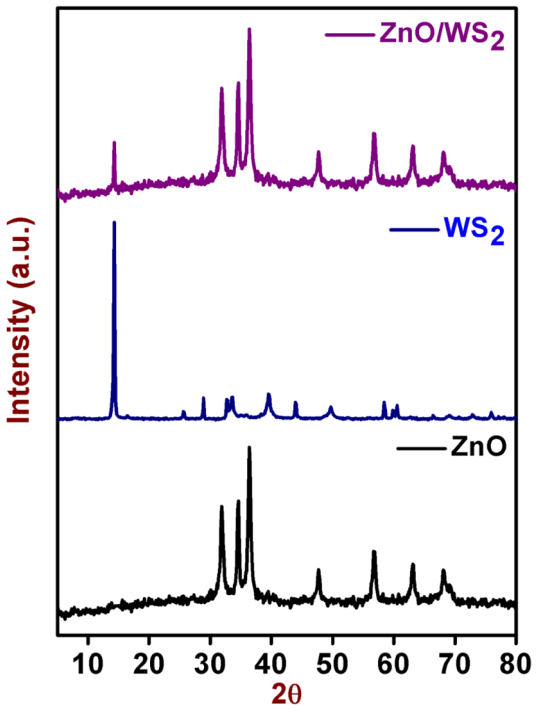

Fig. 1 X-ray diffraction pattern of ZnO, WS_2 and ZnO/WS_2 nanohybrid

successfully formed through the microwave technique without any impurities.

Further, to understand the surface morphology of pure ZnO, WS_2 and ZnO/WS_2 nanohybrid, SEM analysis was carried out. Figure 2a–d depicts the SEM micrograph of pure ZnO, WS_2 and ZnO/WS_2 nanohybrid. As shown in Fig. 2a, pure ZnO exhibit flakes like structure. Figure 2b shows the plate like structure for WS_2 and in Fig. 2c, d, the ZnO/WS_2 nanohybrid is found to be composed of flake and plate like structure. In addition, to determine the elemental quantity of the bare ZnO and ZnO/WS_2 nanohybrid catalyst, EDS measurement was recorded. Figure 3a–d illustrates the EDS spectrum of ZnO, WS_2, ZnO/WS_2 (5%) and ZnO/WS_2 (10%) nanohybrid. Based on the spectral findings on the pure ZnO and ZnO/WS_2 nanohybrid, it is evident that zinc (Zn), oxygen (O), tungsten (W) and sulphur (S) are present in the hybrid. There were no additional impurities observed in the EDS, which confirms the successful formation of pure ZnO/WS_2 nanohybrid. Further to identify the elemental distribution in ZnO/WS_2 nanohybrid EDS color mapping was measured. Figure 4a represents the SEM micrograph of mapping area of ZnO/WS_2 nanohybrid. Figure 4b shows the overall elemental distribution in the ZnO/WS_2 nanohybrid. Figure 4c–f illustrates the individual color mapping of Zn, O, W and S. The elements in ZnO/WS_2 nanohybrid are uniformly distributed all over the hybrid.

To identify the chemical bonding nature in the ZnO/WS_2 nanohybrid FT-IR spectra was shown in Fig. 5a. The

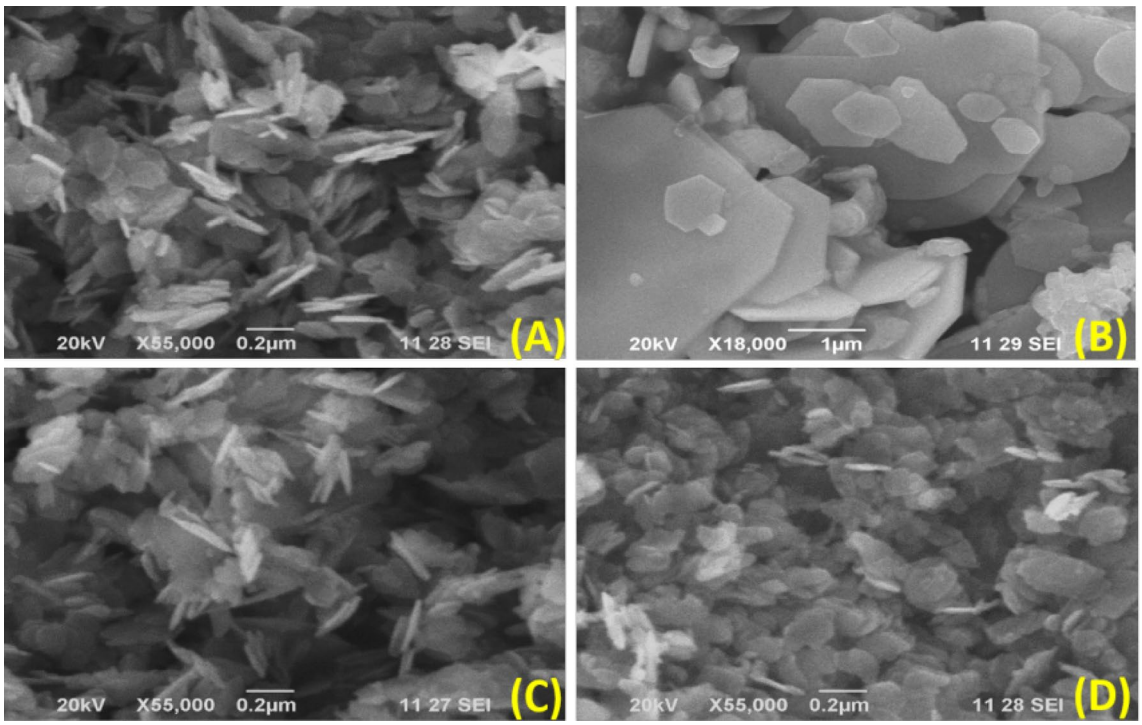

Fig. 2 SEM of **a** ZnO, **b** WS_2, **c** ZnO/WS_2 5% and **d** ZnO/WS_2 10% nanohybrid

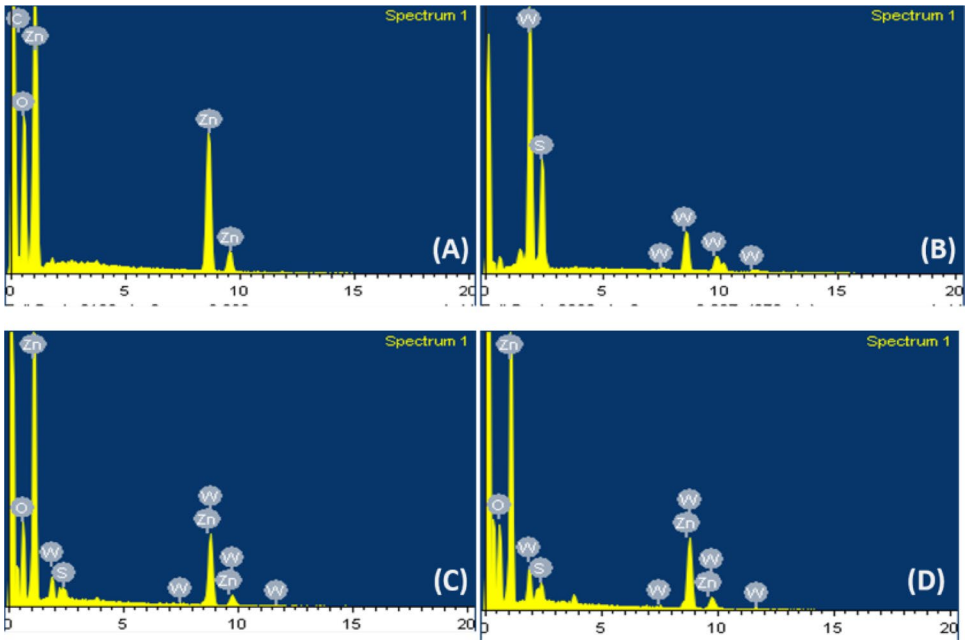

Fig. 3 EDS of **a** ZnO, **b** WS_2, **c** ZnO/WS_2 5% and **d** ZnO/WS_2 10% nanohybrid

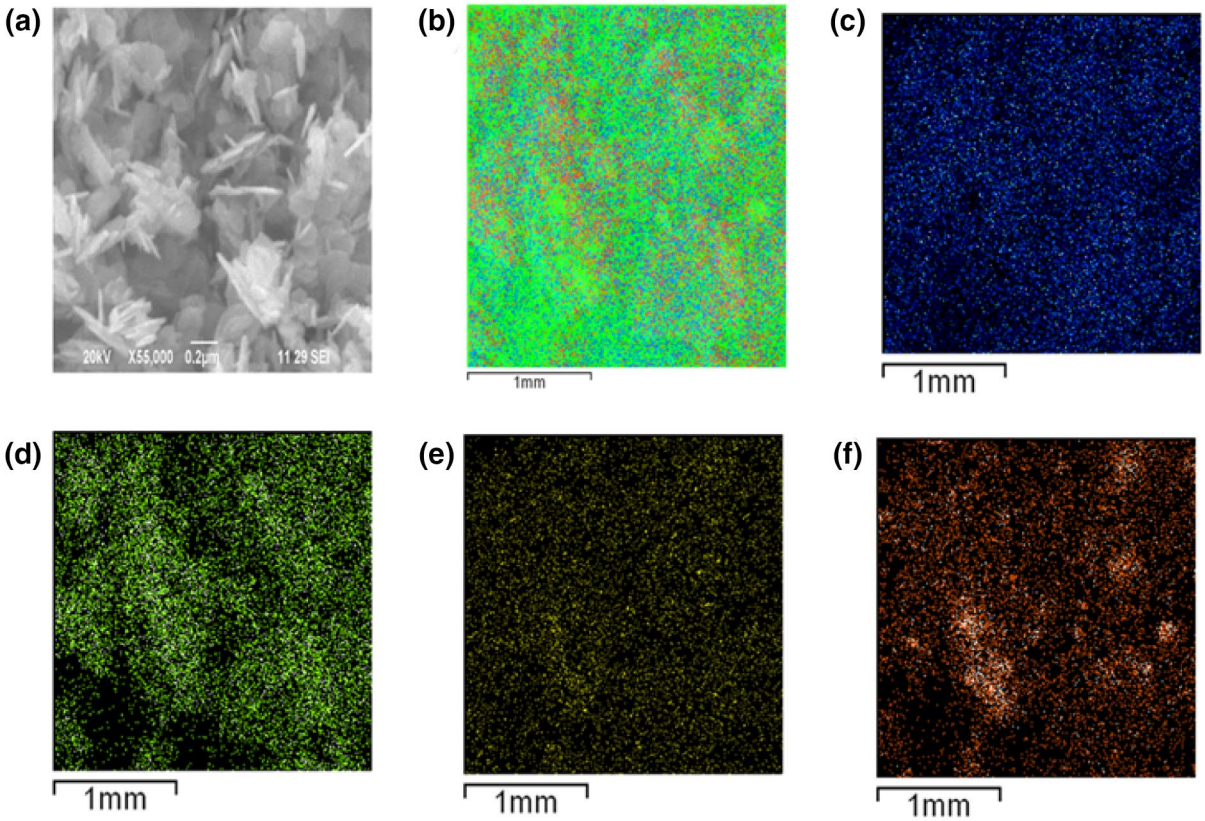

Fig. 4 **a** SEM images of ZnO/WS_2 (20%); energy dispersive mapping of ZnO/WS_2 nanohybrid, **b**–**f** presents the presence of elements Zn, O, W and S which are clearly seen in different colors

FT-IR spectra of the ZnO and ZnO/WS_2 nanohybrid were recorded within the range of 4000–400 cm^{-1}. The major bonds observed were at 3000, 1635, 809 and 442 cm^{-1}. The peak at 3000 cm^{-1} indicates the presence of OH stretching and bending vibrations. These bands indicate the presence of surface adsorbed water molecule in the nanohybrid. The

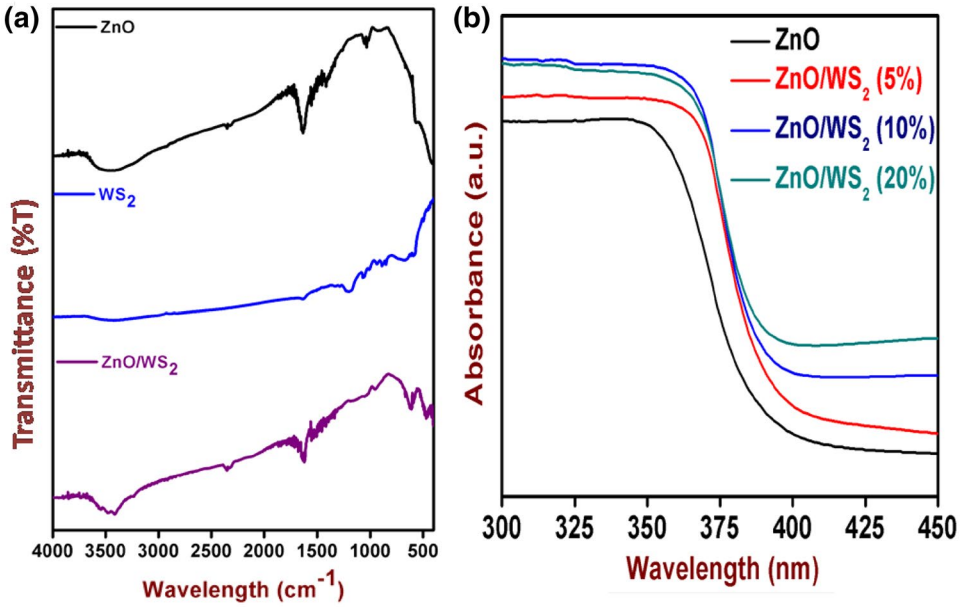

Fig. 5 **a** Fourier transformed infra-red spectra of ZnO, WS_2 and ZnO/WS_2 nanohybrid. **b** Absorbance of ZnO, and ZnO/WS_2 (5%, 10% and 20%) nanohybrids

Zn–O symmetric vibration band located at 809 cm^{-1} and 442 cm^{-1} [25]. In addition, W–S symmetric bending vibration was observed at 577 cm^{-1}, 857 cm^{-1} and 1196 cm^{-1} in ZnO/WS_2 nanohybrid.

The optical property of the ZnO/WS_2 nanohybrid was examined using the UV–DRS technique. The absorbance peak underwent a red shift in the case of ZnO/WS_2 nanohybrid when compared with the peak in bare ZnO. From the UV absorbance spectra the band gap of ZnO/WS_2 nanohybrid was calculated as shown in Fig. 5b. The bare ZnO band gap energy lies in the UV region (3.1 eV), where as a band gap shrink was observed from the UV to the visible region in the case of ZnO/WS_2 nanohybrid. The calculated band gap was found to be around 3, 2.9 & 2.8 eV using the Tauc's plot $((\alpha h\nu)^2/h\nu)$ for the 5%, 10% and 20% loaded ZnO/WS_2 nanohybrid respectively. The band gap reduction observed may be due to the electronic interaction in the ZnO/WS_2 nanohybrid. Increasing the WS_2 loading amount in ZnO/WS_2 nanohybrid, the S^{2-} ions create oxygen vacancies in the ZnO structure [26]. These defects are the main reason for enhancing the visible-light activity. Further, to investigate the optical properties of the ZnO/WS_2 nanohybrid the PL spectroscopy study was carried out. PL is a widely used technique to characterize the optical and electronic properties of the semiconductor. The nature of the zinc interstitial position and the oxygen vacancy of the ZnO semiconductor were analyzed from the PL study. Figure 6a shows the PL spectra of the prepared ZnO, and ZnO/xWS_2 (x = 5, 10 and 20%) nanohybrid. The PL spectra of the prepared ZnO/WS_2 nanohybrid, was analyzed with respect to the excitation wavelength of 320 nm. The peak observed at 490 nm is due to the formation of oxygen-related defects in the ZnO nanostructures. By increasing the loading amount of WS_2 in the ZnO/WS_2 nanohybrid, the PL intensity was found to decrease. The decrease in intensity clearly shows that in the ZnO/WS_2 nanohybrid the electron–hole recombination process is minimized [27].

In order to understand the valance and conduction band position in the ZnO/WS_2 nanohybrid, the Mott–Schottky analysis was performed. The Mott–Schottky measurement was conducted in 0.5 M Na_2SO_4 aqueous solution at pH 7 under dark condition. The flat band potentials of ZnO/WS_2 nanohybrids were determined using the Mott–Schottky expression at 298 K. The estimated flat band potential was found from the average value of the *x*-intercepts of the linear portion of the Mott–Schottky plot. The determined flat band potential was found to be − 1.01, − 0.89 & − 0.74 for ZnO/WS_2 (5%), ZnO/WS_2 (10%), ZnO/WS_2 (20%) nanohybrid respectively. The measured potentials versus the Ag/AgCl were converted to the reversible hydrogen electrode (RHE) scale via the Nernst equation [28]:

$$V_{RHE} = V_{\mathrm{Ag/AgCl}} + V^{0}_{\mathrm{Ag/AgCl}\ vs.\ NHE} + 0.059 \times \mathrm{pH} \quad (4)$$

Here V_{RHE} is the converted potential versus RHE, $V_{\mathrm{Ag/AgCl}}$ is the experimental potential measured against Ag/AgCl reference electrode and the $V^{0}_{\mathrm{Ag/AgCl}\ vs.\ NHE}$ is 0.209 V at 25 °C. Figure 7a–c illustrates the flat band potential of ZnO/WS_2 loaded with 5%, 10% and 20% of WS_2. Using the above mentioned expression, the positions of the conduction band of the 5, 10 and 20% ZnO/WS_2 nanohybrid were calculated and found to be at − 0.388 V_{RHE}, − 0.268 V_{RHE} and − 0.118 V_{RHE} respectively. Based on the band gap and Mott–Schottky analysis, position of the valence and conduction band is shown in Fig. 7d.

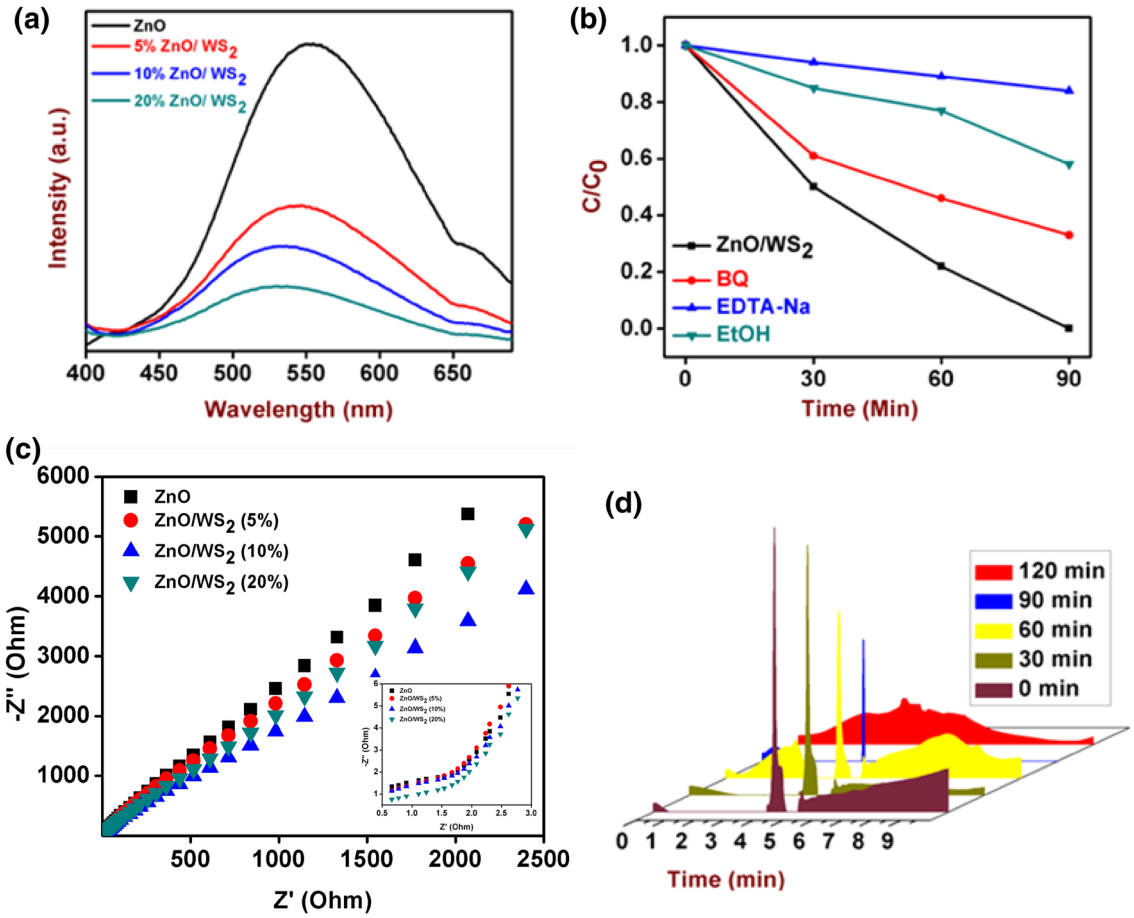

Fig. 6 **a** Room temperature PL spectra of ZnO/WS_2 nanohybrids (5, 10 and 20%). **b** Effect of scavenger on MB photodegradation by ZnO/WS_2 nanohybrids. **c** Impedance spectra of ZnO/WS_2 nanohybrids (5, 10 and 20%). **d** High-performance liquid chromatography analysis of MB by photodegradation by ZnO/WS_2 nanohybrids

3.1 Photocatalytic measurement and analysis

The photocatalytic activity of the as prepared bare ZnO and ZnO/WS_2 nanohybrids is measured by the photocatalytic degradation of the azo dye MB, BP and a phenolic compound like 4-NP. Azo dyes are frequently used in textiles as a coloring agent and are highly environmentally toxic due to their carcinogenic effect. The UV absorbance spectra of MB showed a strong and shoulder peak at 664.5 nm and 292 nm due to the hetero-polyaromatic and benzene. BPB is a triphenylmethane derivative which has been used in foods, drugs and cosmetics as a coloring agent and is environmentally carcinogenic and genotoxic. BPB exhibits a strong absorbance peak at 590 nm [29]. Likewise 4-NP has a strong absorbance peak at 405 nm. All the three compounds are highly stable under biodegradation and light. The photocatalytic degradation of MB, BPB and 4-NP were carried out by ZnO, ZnO–WS_2 nanohybrids. Initial, control experiments were performed to ensure the difference between the photodegradation reactions in the absence of light and catalyst. There is no significant change observed in MB UV–Vis spectra in the following reactions (i) absence of light and (ii) absence of the catalyst. These reactions ensured that the reaction is not accelerated by self-oxidation. The MB and BP photodegradation was studied in the presence of light and ZnO–WS_2 nanohybrid. The corresponding UV absorbance spectra is shown in Fig. 8a, c, e. The absorbance intensity was decreased due to the synergetic photocatalytic effect of the ZnO–WS_2 nanohybrid. Probe concentration changes ratio is directly proportional to the absorbance of the dye at regular time period. The photocatalyst decolorization of MB, BPB and 4NP in the presence of ZnO–WS_2 nanohybrid follows the pseudo-first-order reaction kinetics, provided by the Langmuir–Hinshelwood mode. Figure 8b, d, f shows the plot of $\ln(C/C_0)$ against irradiated time 't' for the MB and the BPB, catalyzed by ZnO and the ZnO/WS_2 nanohybrid. The photodecolorization efficiency of ZnO/WS_2 is about 100% for the photodegradation of MB, similarly BPB degradation efficiency is about 96% with the ZnO/WS_2 nanohybrid catalyst. The 4NP degradation efficiency reached 92%

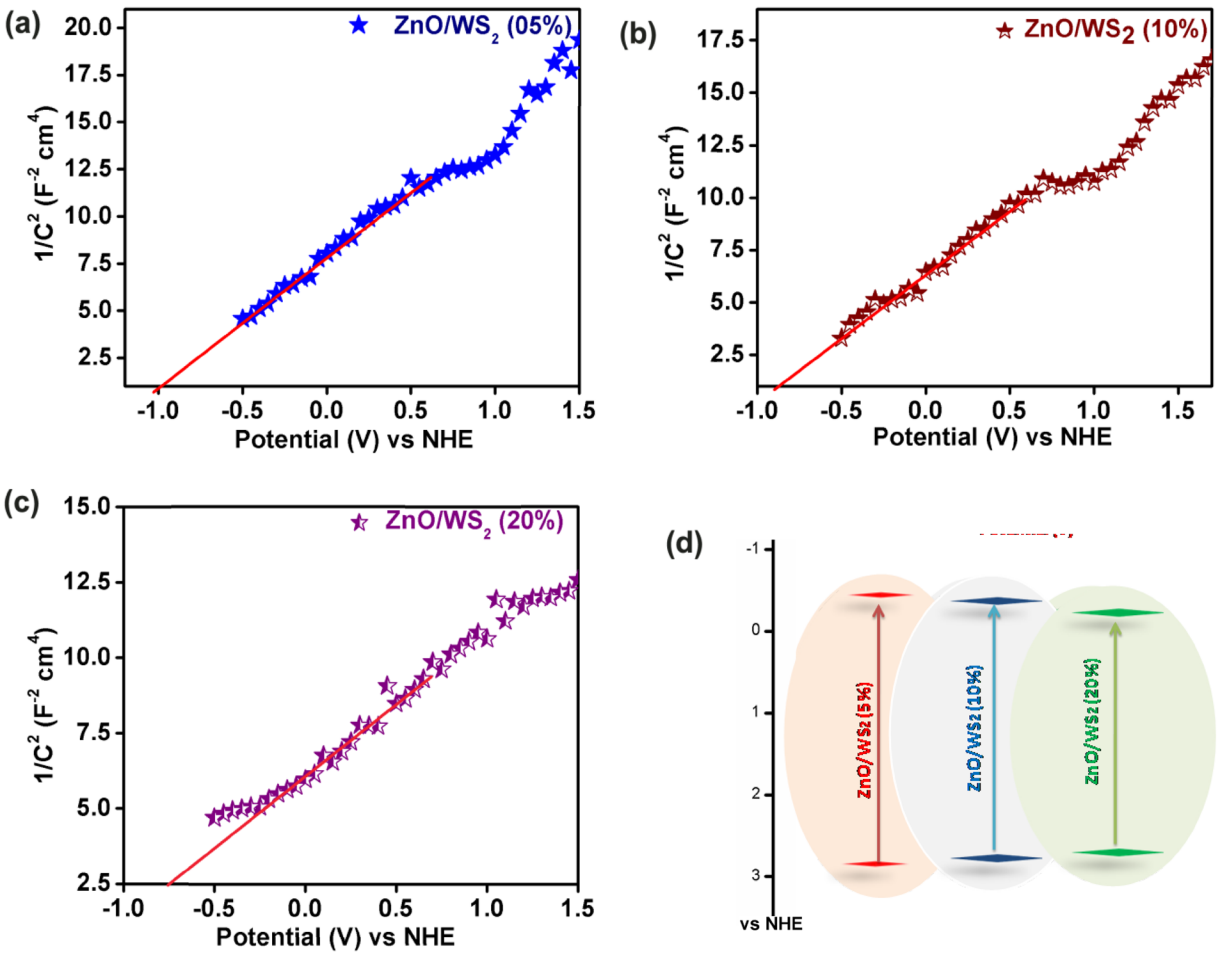

Fig. 7 Mott–Schottky plot of **a** ZnO/WS_2 5%, **b** ZnO/WS_2 10%, **c** ZnO/WS_2 20%, and **d** band potential of ZnO/WS_2 (5%, 10% and 20%)

in the presence of the ZnO/WS_2 nanohybrid catalyst. The pseudo-first-order rate constant of MB catalyzed by ZnO and $ZnO–WS_2$ is found to be 0.0016 and 0.0106. The pseudo-first-order reaction constant k is 6.6-fold higher when compared with the bare ZnO in the photo decolorization of MB. Likewise, the rate constant k is 0.0018 increased when compared with bare ZnO in the photo decolorization of the BPB. From the photodecolorization study of MB, BPB and 4NP, it is understood that the superior photocatalytic efficiency achieved in the case of $ZnO–WS_2$ nanohybrid, is due to the synergistic effect. In addition, we examined the effect of WS_2 loading in the $ZnO–WS_2$ nanohybrid. The $ZnO–WS_2$ nanohybrid loaded with 5%, 10% and 20% of WS_2 were studied for their photocatalytic activity to understand the influence of WS_2 in the nanohybrid. Figure 9a represents the plot of concentration changes against irradiation time 't' and the calculated efficiency was 73.6%, 96.6%, 99.6% for the weight ratio 5%, 10% and 20% respectively. The results ensured that 20% WS_2 loaded $ZnO–WS_2$ nanohybrid exhibits its enhanced photocatalytic activity. When decreasing the WS_2 concentration to 5% and 10% of $ZnO–WS_2$ results in a decrease in the photocatalytic efficiency. Figure 9b illustrates the MB degradation in the presence of WS_2/ZnO using natural sunlight. The hybrid nanomaterial was found to be highly active in natural sun light condition. The degradation of MB under this condition was observed to be around 99%.

The experimental analysis showed that $ZnO–WS_2$ nanohybrid possesses improved efficiency when compared with the bare ZnO. This enhanced photocatalytic efficiency can be attributed to the creation of electron–hole pair in the ZnO semiconductor during the absorption of energy photon. The produced charge carrier, further under goes the reaction with water, and oxygen, which in turn produces reactive oxygen species such as superoxide and hydroxyl radical. The free radicals decompose the organic dye molecule into CO_2 and H_2O. Meanwhile, the electron and hole recombination leads to decrease in the efficiency. The electron–hole recombination was decreased with the addition of WS_2 into the $ZnO–WS_2$ nanohybrids. Therefore more production of reactive oxygen species results which in turn increases the efficiency. In order to evaluate this electron hole recombination process, PL spectra was measured for bare ZnO and

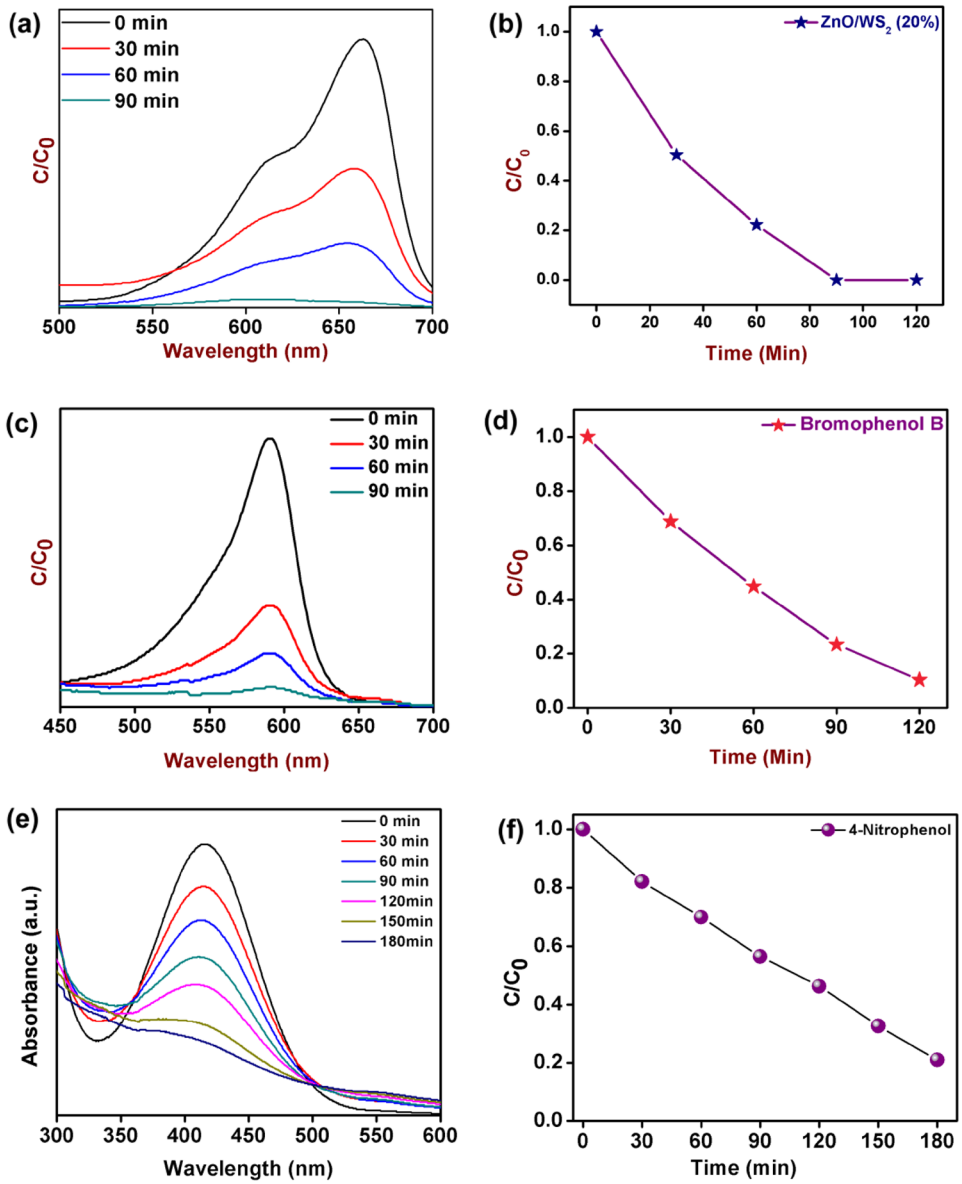

Fig. 8 Photocatalytic performance of ZnO/WS_2 nanohybrids over the degradation of **a** MB, **c** BPB and **e** 4-NP measured by UV–Vis spectroscopy. Rate kinetics of **b** MB, **d** BPB and **f** 4-NP photodegradation by ZnO/WS_2 nanohybrids

$ZnO–WS_2$ nanohybrid with different wt% additions of WS_2 like 5%, 10% and 20% at a excitation wavelength of 320 nm. Figure 6a represents the PL spectra of ZnO and $ZnO–WS_2$ with different quantities of WS_2 like as 5%, 10% and 20%. Bare ZnO exhibits a broad emission at 560 nm due to the zinc and oxygen vacancies and electron–hole recombination. The emission intensity is quenched in $ZnO–WS_2$ nanohybrid when compared with ZnO and the quenching is enhanced by adding 5%, 10% and 20% of WS_2 into the ZnO. The quenching is observed due to the transfer of photo generated electron from ZnO to WS_2 as observed in graphene and MoS_2. Moreover, the good conductive nature of the WS_2 sheet, acts as a good platform to access the photo induced electron. The trapped photo induced electron reacts with the dissolved oxygen to form the superoxide radicals. Hydroxyl radical is formed by the reaction of OH and a hole from the valence band of ZnO. This superoxide and hydroxyl radicals decomposes the organic dye. Further we examined the effect of free radical scavenger to understand the dominant free radicals such as electron, hole, super oxide, hydroxyl and singlet oxygen. Figure 6b shows the MB degradation with the addition of various scavengers like EDTA-Na, benzoquinone and ethanol. The photocatalytic reaction efficiency was found to highly decrease by adding EDTA-Na and slightly disturbed by the BQ and ethanol addition [30]. The scavenger study indicates that, MB photodegradation is mainly driven by the singlet oxygen. Figure 6c illustrates the Nyquist plot of ZnO/WS_2 nanohybrids. When different wt% (5%, 10% and 20%) of WS_2 was added into the ZnO, the Nyquist plot is decreased. This shows that the 20% addition of WS_2 brought

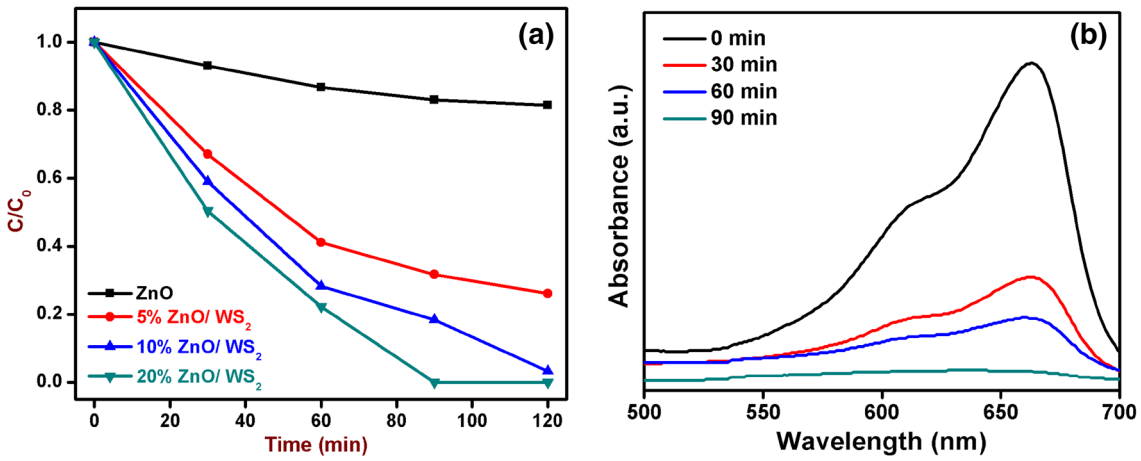

Fig. 9 Photocatalytic performance of ZnO and ZnO/WS_2 (5%, 10% and 20%) nanohybrids over the degradation of **a** MB rate kinetic and **b** MB degradation of ZnO/WS_2 20% nanohybrid using natural sun light

about more effective separation of photogenerated charge carrier due to its smaller arc [31]. In addition, the degradation reaction was analyzed with HPLC which is shown in Fig. 6d. The peak intensity associated with MB was found to decrease with respect to the time of irradiation. Moreover, the appearance of small new peaks indicate the formation of new photocatalytic products. The entire ZnO/WS_2 nanohybrid photocatalytic mechanism is given in Fig. 10.

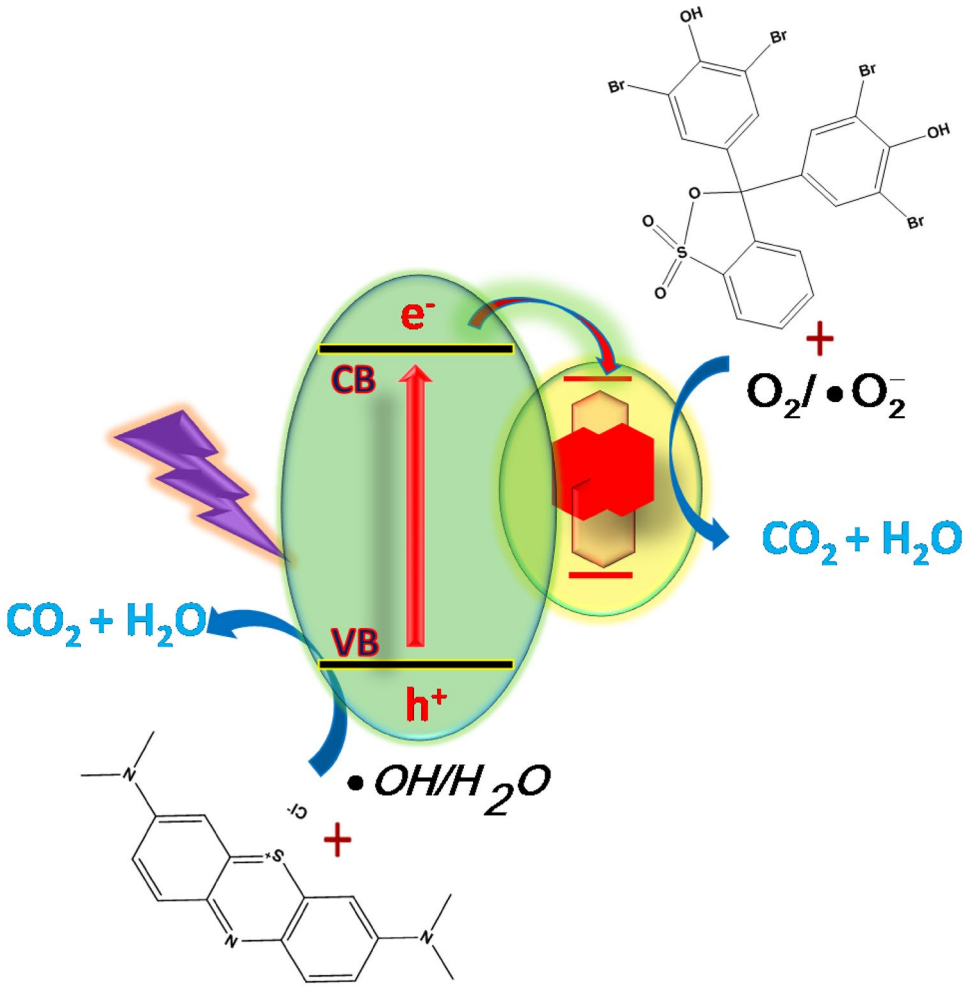

Fig. 10 Schematic diagram for ZnO/WS_2 photocatalytic degradation mechanism

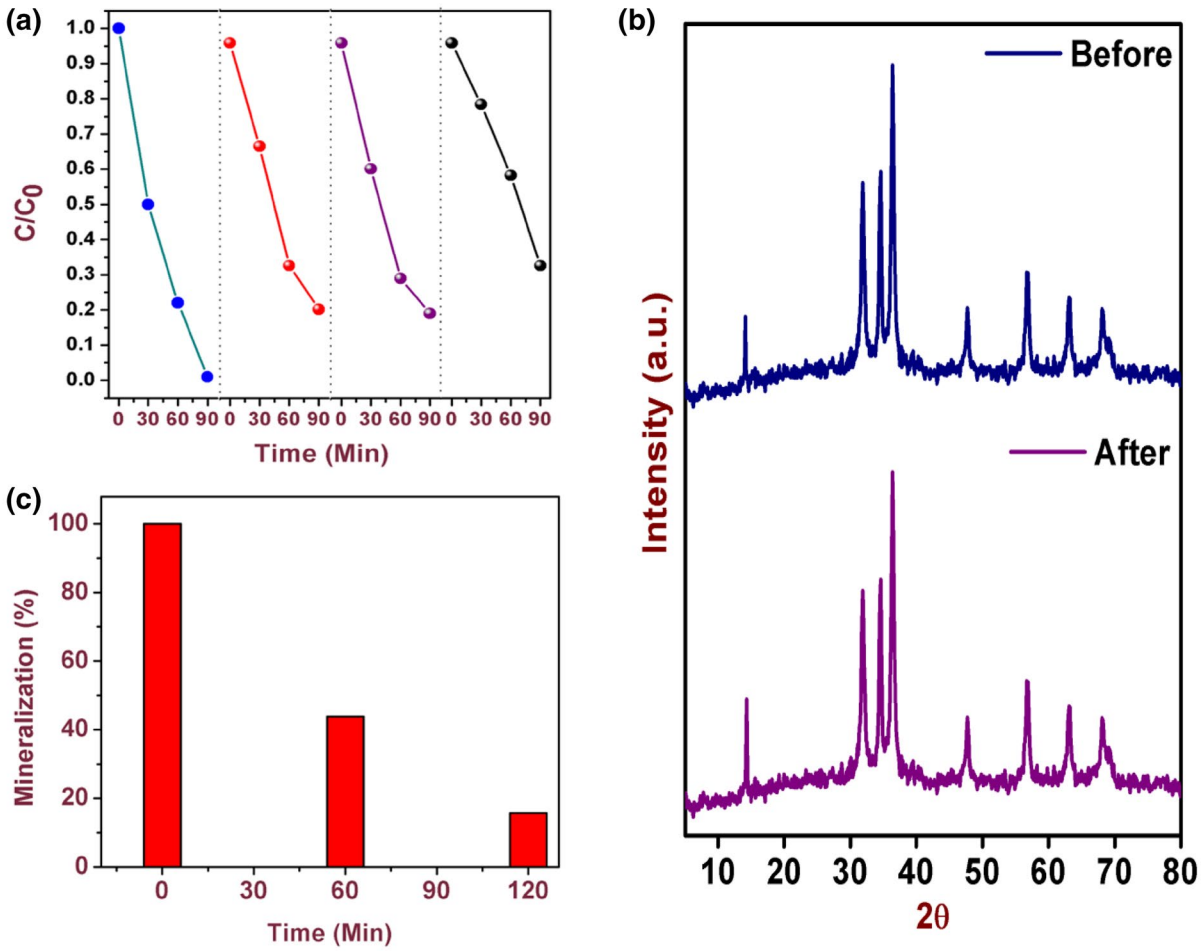

Fig. 11 **a** MB photodegradation by ZnO/WS_2 nanohybrids over four conservative cycles. **b** XRD pattern of ZnO/WS_2 after the cycle test. **c** TOC removal efficiency MB by photodegradation by ZnO/WS_2 nanohybrids

An ideal photocatalyst should be tested for consecutive photocatalytic cyclic test. To examine the recyclability of the ZnO/WS_2 nanohybrid catalyst, a recycle study was performed. Figure 11a reveals that there is no significant loss of catalytic efficiency observed even in the fourth successive cycle. Further, the structure and phase of the ZnO/WS_2 were investigated after the photocatalytic degradation. Figure 11b represents the XRD pattern ZnO/WS_2 nanohybrid reused catalyst. The diffraction results confirmed that there were no obvious changes observed in the ZnO/WS_2 nanohybrid after the recycle. In addition, TOC measurement was carried out for the mineralization of MB in the presence of ZnO/WS_2 nanohybrid. 80% of MB mineralization was achieved using the ZnO/WS_2 nanohybrid which is shown in Fig. 11c.

4 Conclusion

In conclusion, we have successfully synthesized ZnO and ZnO/WS_2 nanohybrid with Nano flakes morphologies using Microwave techniques. The phase and microstructural information of the ZnO and ZnO/WS_2 nanohybrid was studied using the XRD, SEM/EDS, EDS color mapping and FTIR spectroscopy techniques. The powder XRD, SEM and FT-IR results corroborate the formation of crystalline ZnO and ZnO/WS_2 nanohybrid. The ZnO/WS_2 nanohybrid exhibits better catalytic property in visible light conditions as confirmed by the UV–DRS study. The MB, BPB and 4-NP degradation results confirmed that the ZnO/WS_2 nanohybrid exhibits improved photocatalytic efficiency due to the synergistic effect of ZnO and WS_2 Moreover, along with the efficiency enhancement, the band gap reduction and a high conductive nature of the ZnO/WS_2 nanohybrid was observed. The catalyst demonstrates better mineralization efficiency. The recycle and phase analysis studies indicate

that the catalyst has good durability even up to the fourth cycle. All the results put together reveals that the ZnO/WS_2 nanohybrid catalyst can be used as a potential catalytic material for environmental remediation.

Acknowledgements The authors are grateful to the Management and the Authorities of Karunya Institute of technology and science, Coimbatore, for their valuable support and constant encouragement. The authors are grateful to the Department of Science and Technology, Govt of India for their financial support.

References

1. G. Wang, H. Wang, Y. Ling, Y. Tang, X. Yang, R.C. Fitzmorris, C. Wang, J.Z. Zhang, Y. Li, Nano Lett. **11**, 3026 (2011)
2. M.M. Khan, S.F. Adil, A. Al-Mayouf, J. Saudi Chem. Soc. **19**, 462 (2015)
3. P.V. Kamat, J. Phys. Chem. Lett. **1**, 520 (2010)
4. X. Hu, G. Li, J.C. Yu, Langmuir **26**, 3031 (2010)
5. H.L. Tan, A. Du, R. Amal, Y.H. Ng, Chem. Eng. Sci. (2017). https://doi.org/10.1016/j.ces.2017.12.042
6. N. Raghavan, S. Thangavel, G. Venugopal, Mater. Sci. Semicond. Process. **30**, 321 (2015)
7. D. Zhao, G. Sheng, C. Chen, X. Wang, Appl. Catal. B **111–112**, 303 (2012)
8. S. Thangavel, S. Thangavel, N. Raghavan, R. Alagu, G. Venugopal, J. Phys. Chem. Solids **110**, 266 (2017)
9. A. Durairaj, T. Sakthivel, A. Obadiah, S. Vasanthkumar, J. Mater. Sci. Mater. Electron. **29**, 8201 (2018)
10. X. Huang, Z. Zeng, H. Zhang, Chem. Soc. Rev. **42**, 1934 (2013)
11. W. Choi, N. Choudhary, G.H. Han, J. Park, D. Akinwande, Y.H. Lee, Mater. Today **20**, 116 (2017)
12. B. Ji, J. Zhang, C. Zhang, N. Li, T. Zhao, F. Chen, L. Hu, S. Zhang, Z. Wang, ACS Appl. Nano Mater. **1**, 793 (2018)
13. B. Mahler, V. Hoepfner, K. Liao, G.A. Ozin, J. Am. Chem. Soc. **136**, 14121 (2014)
14. L. Zheng, W. Zhang, X. Xiao, Korean J. Chem. Eng. **33**, 107 (2016)
15. K.M. Lee, C.W. Lai, K.S. Ngai, J.C. Juan, Water Res. **88**, 428 (2016)
16. C. Feng, Z. Chen, W. Li, J. Zhou, Y. Sui, L. Xu, M. Sun, J. Mater. Sci. Mater. Electron. **29**, 9301 (2018)
17. S.-M. Lam, J.-C. Sin, A.Z. Abdullah, A.R. Mohamed, Desalin. Water Treat. **41**, 131 (2012)
18. F. Wang, W. Li, S. Gu, H. Li, X. Liu, M. Wang, ACS Sustain. Chem. Eng. **4**, 6288 (2016)
19. S. Thangavel, K. Krishnamoorthy, V. Krishnaswamy, N. Raju, S.J. Kim, G. Venugopal, J. Phys. Chem. C **119**, 22057 (2015)
20. G.P. Awasthi, S.P. Adhikari, S. Ko, H.J. Kim, C.H. Park, C.S. Kim, J. Alloys Compd. **682**, 208 (2016)
21. F. Guo, W. Shi, W. Guan, H. Huang, Y. Liu, Sep. Sci. Technol. **173**, 295 (2017)
22. J. Wang, L. Tang, G. Zeng, Y. Liu, Y. Zhou, Y. Deng, J. Wang, B. Peng, ACS Sustain. Chem. Eng. **5**, 1062 (2017)
23. Y. Xu, J. Jin, X. Li, Y. Han, H. Meng, T. Wang, X. Zhang, Mater. Res. Bull. **76**, 235 (2016)
24. B. Mahler, V. Hoepfner, K. Liao, G.A. Ozin, J. Am. Chem. Soc. **136**, 14121 (2014)
25. M. Zare, K. Namratha, K. Byrappa, D.M. Surendra, S. Yallappa, B. Hungund, J. Mater. Sci. Technol. **34**, 1035 (2018)
26. X. Zhang, F. Qiu, X. Rong, J. Xu, J. Rong, T. Zhang, Can. J. Chem. Eng. **96**, 1053 (2018)
27. H. Mou, C. Song, Y. Zhou, B. Zhang, D. Wang, Appl. Catal. B **221**, 565 (2018)
28. C.-J. Chang, K.-L. Huang, J.-K. Chen, K.-W. Chu, M.-H. Hsu, J. Taiwan Inst. Chem. Eng. **55**, 82 (2015)
29. H. Khan, A.K. Khalil, A. Khan, K. Saeed, N. Ali, Korean J. Chem. Eng. **33**, 2802 (2016)
30. Q. He, Y. Ni, S. Ye, RSC Adv. **7**, 27089 (2017)
31. C. Xia, Z. Qiao, C. Feng, J.-S. Kim, B. Wang, B. Zhu, Materials **11**, 40 (2017)